



# Modifying the microstructure of chitosan/methylcellulose polymer blend via magnesium nitrate doping to enhance its ionic conductivity for energy storage application

Pradeep Nayak · Y. N. Sudhakar · Shounak De ·  
Ismayil · Supriya K. Shetty · Vipin Cyriac

Received: 19 October 2022 / Accepted: 22 February 2023 / Published online: 21 March 2023  
© The Author(s) 2023

**Abstract** In this study, different weight percentages of  $Mg(NO_3)_2$  were added to a polymer blend composed of chitosan (CS) and methylcellulose (MC). The solution casting method was adopted to prepare the polymer electrolyte films. As the host matrix, the polymer blend consists of 70 wt.% of CS and 30 wt.% of MC. The interactions between the blend and the  $Mg(NO_3)_2$  salt were revealed by FTIR analysis. The deconvolution of XRD peaks followed by the calculation of crystallinity indicates that the electrolyte samples were amorphous. The bulk resistance decreased with increasing salt content, according to the results of electrical impedance spectroscopy (EIS), and this

was caused by the influence of carrier concentration. The sample containing 30 wt.% of  $Mg(NO_3)_2$  was determined to have a maximum value of DC conductivity of  $2.12 \times 10^{-5} \text{ Scm}^{-1}$  at room temperature by EIS analysis. The highest conducting film's potential stability was found to be 3.65 V. It was found that the ion transference number was 0.86. The performance of the magnesium ion battery was then evaluated after it was built using the highest conducting polymer electrolyte. Considering this, the current work proposes an eco-friendly, practical, and affordable electrolyte appropriate for making electrochemical devices.

---

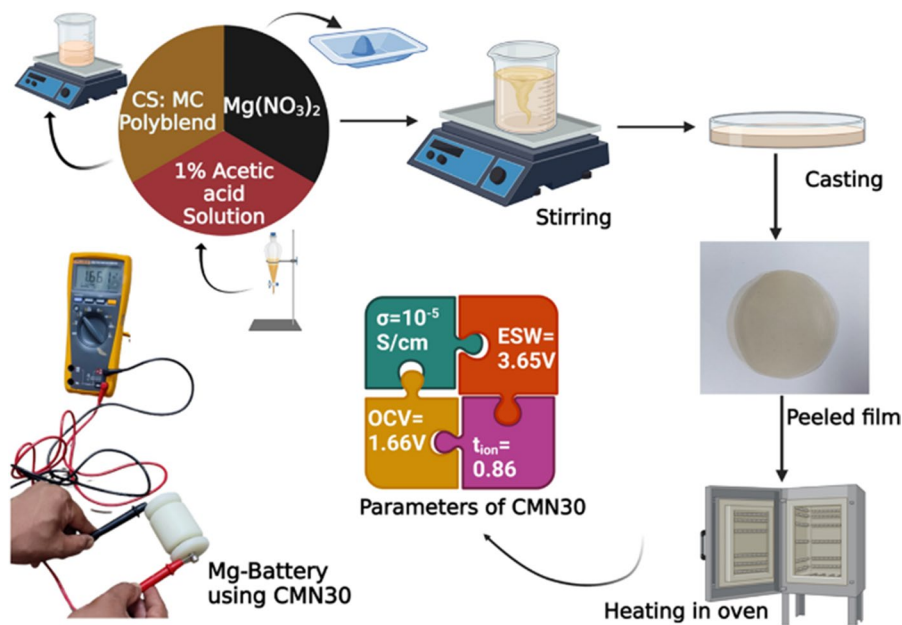
P. Nayak · S. K. Shetty · V. Cyriac  
Department of Sciences, Manipal Academy of Higher  
Education, Manipal 576104, Karnataka, India

P. Nayak · Ismayil (✉) · S. K. Shetty · V. Cyriac  
Department of Physics, Manipal Institute of Technology,  
Manipal Academy of Higher Education, Manipal 576104,  
Karnataka, India  
e-mail: ismayil.mit@manipal.edu; ismayil.486@gmail.  
com

Y. N. Sudhakar  
Department of Chemistry, Manipal Institute  
of Technology, Manipal Academy of Higher Education,  
Manipal 576104, Karnataka, India

S. De  
Department of Electronics and Communication  
Engineering, Manipal Institute of Technology, Manipal  
Academy of Higher Education, Manipal 576104,  
Karnataka, India

## Graphical abstract (made with biorender.com)



**Keywords** Polymer blend electrolyte · Transport properties · Ionic conductivity · Primary batteries

## Introduction

Electronic appliances such as smartphones, tablets, computers, and other similar devices have become ubiquitous household items, resulting in an increase in demand year after year. Almost all portable electronic devices and electric vehicles contain an energy storage system. Batteries and capacitors are the two main types of energy storage devices. The battery is made up of an anode, a cathode, and an electrolyte. The electrolyte helps transfer ions between the electrodes. A solid-state energy storage device can be constructed by inserting the solid polymer electrolyte between the cathode and anode. The solid polymer electrolyte thus serves as both an electrolyte and a separator (Wang et al. 2017). The advantages of solid polymer electrolytes include their non-volatility, leak-proof nature, wide electrochemical stability window (ESW), and ease of preparation (Khiar et al. 2018).

While lithium batteries can create short circuits due to dendrite formation, magnesium can be

electrodeposited without any dendrite growth (Manjuladevi et al. 2018a, b). Compared to lithium, magnesium is a better choice for use in batteries due to its advantages, such as being less expensive, more prevalent, having a higher energy density, being considerably safer, and being easier to prepare electrodes in an atmosphere filled with oxygen (Manjuladevi et al. 2018a, b). Because of the innate benefits of magnesium metal, magnesium batteries have been proposed as a substitute for next-generation batteries. Properties such as superior ionic conductivity, high ionic transference number, a wide operating temperature range, etc., are desirable in polymer electrolytes for energy storage device applications (Mazuki et al. 2018). Unique properties of biopolymers include their low cost, renewable nature, compatibility with a wide range of solvents, abundance, excellent film formation, and biodegradability. The polymer blend technique can be used to produce a polymer blend with additional sites for ionic conduction (Aziz et al. 2017). Compared to using single polymers, blending polymers is the most effective way to increase ionic conductivity. By blending techniques we can upgrade the properties of individual polymer constituents (Aziz et al. 2020c). The primary benefit of polymer blends

is easy control of physical properties through compositional changes. Blending is also one of the most efficient ways to enhance amorphous content while reducing crystalline content, which is impossible to achieve when utilizing single polymers (Aziz et al. 2020a, b, c; Kesavan et al. 2015). Salman et al. (2018) prepared a polymer electrolyte of CS:MC by incorporating lithium tetrafluoroborate and reported a room temperature conductivity value of  $3.74 \times 10^{-6} \text{ Scm}^{-1}$ . Abdullah et al. (2021b) synthesized a polyblend electrolyte of CS:MC by adding lithium iodide (LiI) as salt and got an ionic conductivity value of  $6.26 \times 10^{-6} \text{ Scm}^{-1}$  for 40 wt.% of LiI salt. Even though Li-salt is thought to be the finest salt for creating polymer-salt complex electrolytes, it has a lot of disadvantages and is only found in small amounts in nature. To find an alternative salt with equivalent electrochemical characteristics, magnesium has been identified as a potential candidate. Researchers have worked on single as well as blended polymers by doping magnesium salts to get polymer electrolyte films. Polu et al. (2013) prepared a polymer electrolyte of poly(vinyl alcohol) (PVA) with  $\text{Mg}(\text{NO}_3)_2$  as salt and obtained an ionic conductivity value of  $7.36 \times 10^{-7} \text{ Scm}^{-1}$ . Manjuladevi et al. (2018a) have synthesized a blend polymer electrolyte by doping 0.3 m.m.%  $\text{Mg}(\text{NO}_3)_2$  with PVA:poly(acrylonitrile) (PAN) which exhibited an ionic conductivity of  $1.71 \times 10^{-3} \text{ Scm}^{-1}$ . Numerous blend electrolytes based on PVA:poly(vinyl pyrrolidone) (PVP), PVA:poly(ethylene glycol) (PEG), and poly(vinylidene fluoride) (PVDF):PVA have also been reported. These blends are made of synthetic polymers, which are detrimental to the environment because they cannot be decomposed easily.

This study is to develop potential magnesium ion conducting solid biodegradable blend polymer electrolytes (SBPEs) for battery applications that contain chitosan (CS) and methylcellulose (MC) as individual polymers. To solvate cations, the polymer used as the matrix needs to have polar groups in its backbone (Aziz et al. 2020b). MC has lone pair electron-containing functional groups such as OH, glycosidic bond, and methoxy groups (Nadirah et al. 2020), whereas CS has functional groups such as amine, OH, and glycosidic (C–O–C) bond groups for ion conduction.

The SBPE system CS:MC has received much attention recently due to its exceptional qualities such as abundance, non-toxicity, environmental

friendliness, and strong film-forming ability (Dannoun et al. 2020; Abdullah et al. 2019; Aziz et al. 2021). Ionic conductivity of  $3.74 \times 10^{-6} \text{ Scm}^{-1}$  was obtained by Salman et al. (2018) by adding lithium tetrafluoroborate to CS:MC blend polymer. Ammonium thiocyanide was used as a dopant by Aziz et al. (2019), who reported that the ionic conductivity of the CS:MC blend electrolyte was  $2.81 \times 10^{-3} \text{ Scm}^{-1}$ . There is very little study on CS:MC blends with magnesium salts, and there have been no studies on  $\text{Mg}(\text{NO}_3)_2$  doped SBPE based on CS:MC for application in magnesium ion batteries.

The present work aims to prepare the biopolymer blend CS:MC with different amount of  $\text{Mg}(\text{NO}_3)_2$  salt by the solution casting technique, and the prepared SBPE were characterized by x-ray diffraction analysis (XRD) which confirms the amorphous nature of the polymer electrolyte, Fourier transform infrared spectroscopy (FTIR) which confirms interaction between the salt and the polymer blend matrix, AC impedance analysis which gives the conductivity and the highest conducting blend polymer electrolyte has been employed in the battery studies which gives an excellent open circuit voltage.

## Experimental

### Materials and method

Chitosan (Viscosity 200 cps), methylcellulose (Viscosity 350–550 cps), graphite (C), and Mg metal powder were procured from Loba Chemie Pvt Ltd.  $\text{Mg}(\text{NO}_3)_2$  salt and acetic acid were procured from S.D. fine-chem. Pvt. limited., Mumbai, India. Manganese dioxide having a molar mass of 86.93 g/mol was procured from Labogens fine Chem, Punjab, India. Iodine ( $\text{I}_2$ ) was obtained from Loba Chemie Pvt. Ltd. All were used as such without any further purification to prepare the SBPE. The polymer electrolyte samples were prepared according to our previous work (Nayak et al. 2022). For a few hours, methylcellulose and chitosan are continuously stirred with a magnetic stirrer in 1% acetic acid solvent to obtain a homogenous solution. The composition of salt and polymers expressed in weight percentage is tabulated in Table 1. with reference to the article (Aziz et al. 2019). The most amorphous blend matrix is one with 70 wt.% of CS and 30 wt.% of MC (Aziz et al.

**Table 1** Sample designation and weight percentage of each component

Sample designation	Polymer CS (g)	Polymer MC (g)	Dopant (Mg(NO <sub>3</sub> ) <sub>2</sub> ) (g)
CMN0	1.44	0.56	–
CMN5	1.33	0.57	0.10
CMN10	1.26	0.54	0.20
CMN15	1.19	0.51	0.30
CMN20	1.12	0.48	0.40
CMN25	1.05	0.45	0.50
CMN30	0.98	0.42	0.60

2020b). Thus, we choose to employ it in this study as the polymer matrix doped with a different weight percentage of Mg(NO<sub>3</sub>)<sub>2</sub> salt varying from 0 to 30 wt.%. To prepare these biopolymer electrolyte complexes, homogenous solutions were carefully cast in Petri dishes and kept in a hot air oven at 60 °C for a few days. The films were then detached from the Petri dishes and kept in a desiccator at room temperature for further analysis. The prepared films had a thickness that varied from 100 to 200 μm.

An Mg (anode)/(CS–MC–Mg(NO<sub>3</sub>)<sub>2</sub>) (70–30–30)/(cathode) electrochemical cell was constructed using the highest conducting SBPE film, and the performance of the cell was studied. Anode preparation: Magnesium metal of diameter 13 mm was used as the anode. Cathode preparation: Iodine (I<sub>2</sub>), graphite (C), and the highest conducting SBPE were mixed and pressed under a 5-ton pressure to make a pellet with a diameter of 13 mm (cell 1), and MnO<sub>2</sub> and C were combined in a 3:1 ratio to produce another pellet (cell 2), both of which were used to analyze the performance of the primary battery.

### Instrumentation

Rigaku Miniflex 600 (5th gen) Cu K<sub>α</sub> (λ = 1.54 Å) radiation was used for XRD studies (14 kV, 15 mA). With a 0.02° step size, the scanning angle range of 2θ was 3° to 80°. XRD is utilized to show the amorphous nature of the polymer electrolyte samples. The FTIR investigations were carried out using a Shimadzu IR spirit ATR-FTIR spectrometer with a resolution of 4 cm<sup>-1</sup> in the wavenumber range of 4000–400 cm<sup>-1</sup>. The complexation between the polymer mixture and the magnesium salt was confirmed using FTIR.

The room temperature electrical conductivity of the SBPE samples was measured utilizing the precision impedance analyzer model number IM 3570, Hioki corporation, Japan, at a frequency range of 100 Hz to 5 MHz with ac voltage of 100 mV. The SBPE was inserted between the two stainless steel blocking electrodes having a contact area of 1.13 cm<sup>2</sup> to measure the real (Z'), imaginary (Z'') part of complex impedance. A field emission scanning electron microscope (CARL ZEISS) at 25 kX magnification was used for microstructural studies. With the use of Keithley source meter 2636B, the SBPE's potential stability was evaluated.

Using the Wagner polarization technique, transference number measurements (TNMs) were done at room temperature using the Keithley source meter 2636B by monitoring the polarization current as a function of time. With the cell arrangement, Mg | CMN30 | Mg, between –1 V and +1 V, and a scan rate of 100 mV/s, a cyclic voltammogram was recorded using a potentiostat (CH Instruments model 600E series).

## Results and discussion

### XRD analysis

Figure 1 illustrates the x-ray diffraction pattern of pure blend and Mg salt-doped polymer electrolyte films. The XRD peak of CS occurs at 11° and 20° (Khar 2018). For MC, the typical peaks will be around 8.5° and 20° (Aziz et al. 2020a; Abdullah et al. 2021a). It should be noted that two distinct concave peaks can be seen from the XRD pattern of the CS:MC system (see Fig. 1). All these peaks were

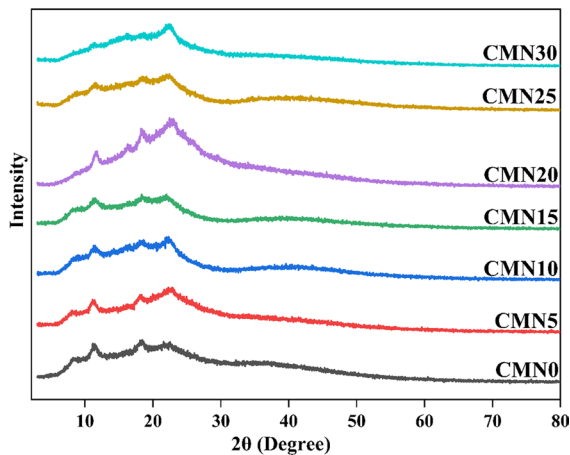


**Fig. 1** XRD pattern for pristine and poly-blend doped with various amounts of  $Mg(NO_3)_2$

superimposed with the amorphous hump background. The XRD pattern of the blend consists of the contribution from the CS and MC. Therefore, on deconvolution, the contribution from both components has to be considered. Thus, the peak assignments have been assigned by considering the crystalline peaks of the components. The blending of MC with CS reduces the crystalline nature of CS because of the strong interaction of MC with the CS and disrupting the hydrogen bonding of CS (Kumari et al. 2012; Liu et al. 2013; Kanimozhi et al. 2016). It is well known that ion migration occurs through the amorphous region, and higher amorphosity means easier ion migration (Arya and Sharma 2019). Earlier research on polymeric systems indicated that an increase in the broadness of the XRD peak suggests an increase in the amorphous fraction (Bdewi et al. 2016; Kumar et al. 2015). Intramolecular interactions between  $Mg^{2+}$  and functional groups in both CS and MC chains, as evident from FTIR studies, diminish the crystallinity of the PE system at low salt concentrations.

The XRD peaks were deconvoluted utilizing Fityk computer software (Wojdyr et al. 2004), and according to the equation

$$X_c = \frac{A_c}{A_a + A_c} 100\% \quad (1)$$

where  $A_c$  and  $A_a$  indicate the area under the crystalline peak and amorphous peak, respectively, as shown in Fig. 2 (a–g). The computed values of the degree of crystallinity of different poly-blend electrolyte

systems are shown in Fig. 2 (h). The calculated values of the degree of crystallinity of the different polymer electrolyte systems indicate that these samples are amorphous in nature, and this facilitates ion conduction.

### FTIR study

FTIR measurements were carried out to confirm the interactions between the CS: MC blend polymers and the  $Mg(NO_3)_2$  salt (Sownthari and Suthanthiraraj 2013). Complexation occurs when the functional groups in the polymer matrix and metal salt ions coordinate. If complexation has occurred, this interaction will change/shift the intensity of the absorption band, which will influence the local structure of the polymer backbone and the active infrared modes of vibration (Manjuladevi et al. 2018a). The C–O bond in ether was found to have a bending peak around  $1057\text{ cm}^{-1}$  for MC polymer (Aziz et al. 2020b).

The peak at  $1026\text{ cm}^{-1}$  in the IR spectra corresponds to the C–O stretch in the polymer backbone. A peak around  $2900\text{ cm}^{-1}$ , is associated with the C–H stretching mode. This peak is then shifted towards a higher wavenumber when the salt concentration is raised, which explains the interaction between the C–H of polymer and  $NO_3^-$  of salt. The C=O (amide I) stretching and -NH (secondary amide II) bending bands are located at  $1641\text{ cm}^{-1}$  and  $1550\text{ cm}^{-1}$ , respectively, in the blended film's spectra, as shown in Fig. 3. Table 2 lists these band positions, which are almost identical to those reported in other investigations (Wang et al. 2017; Buraidah and Arof 2011; Kadir et al. 2011). The absorption band caused by -OH stretching is found in a broad peak form at  $3626\text{--}3132\text{ cm}^{-1}$ , arising from adding salt to the system. The doping has brought about a significant change in the band position as well as in the band structure with a prominent shift in the -OH peak (Jeyabanu et al. 2018). It may be deduced from these FTIR investigations that the  $Mg(NO_3)_2$  salt and the CS:MC blend have formed a complex. The formation of the ion dipole between the  $NO_3^-$  anion with the C–H group has resulted in the shift in peak corresponding to C–H stretching. The band observed at  $1411\text{ cm}^{-1}$  corresponds to -CH<sub>2</sub> bending and the peak at  $1379\text{ cm}^{-1}$  ascribed to CH<sub>3</sub> symmetrical deformation of chitosan polymer (Lawrie et al. 2007). FTIR spectra of  $Mg(NO_3)_2 \cdot 6H_2O$  salt exhibits

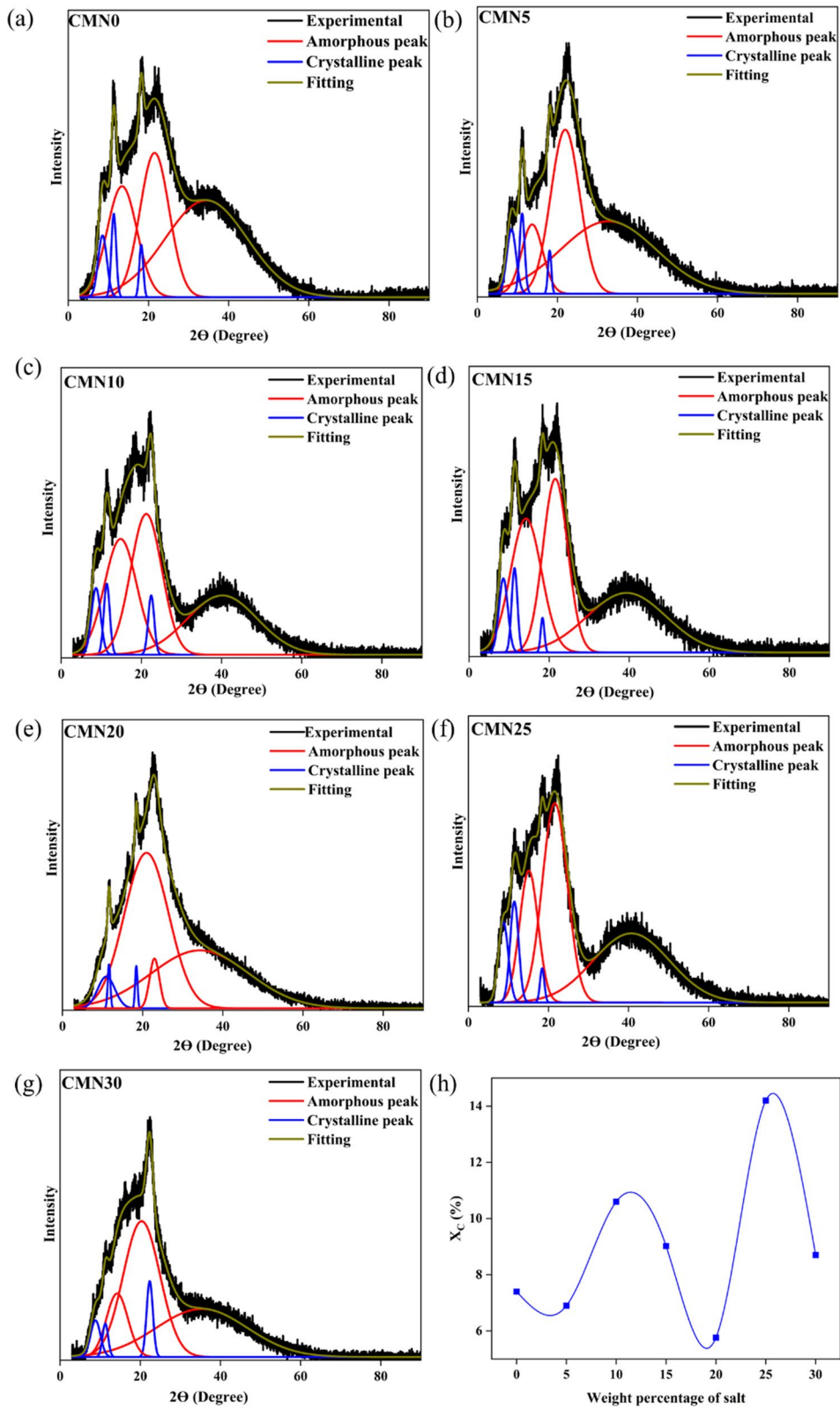




**Fig. 2** (a)–(g) XRD deconvoluted pattern for different poly-blend electrolyte systems and (h) variation of percentage of crystallinity with weight percentage of the salt

bands at  $3347\text{ cm}^{-1}$  that corresponds to  $-OH$  stretching, band at  $1647\text{ cm}^{-1}$  ascribed to  $N = O$  bending, a prominent broad band at  $1351\text{ cm}^{-1}$  corresponds to combined effect of  $N = O$  bending and  $N - O$  stretching and a band at  $818\text{ cm}^{-1}$  corresponds to out of plane deformation mode of  $NO_3^-$  (Graham et al. 2016).

The  $Mg(NO_3)_2$  salt's possible interaction with the poly-blend is shown in Fig. 4.  $Mg^{2+}$  acts as Lewis acid, and  $NO_3^-$  act as Lewis base. The shift in the wavenumber of the  $-OH$  band indicates the formation of ion–dipole  $Mg^{2+} \cdots \cdots OH$  complex (Fig. 4). A Lewis acid–base adduct, a compound that contains a coordinate covalent bond between the Lewis acid and the Lewis base is formed. The interaction between two polymers in a polymer blend is caused by hydrogen bonding (Nadirah et al. 2020).

#### Transport parameters

To understand the prominent parameters that have influenced the ionic conductivity in the electrolyte transport parameters: charge density ( $\eta$ ), Ionic mobility ( $\mu$ ), and diffusion coefficient ( $D$ ) are evaluated from FTIR deconvolution technique using non-linear fitting software. For the FTIR deconvolution, the region between  $1200$  to  $1500\text{ cm}^{-1}$  has been chosen since the peak at  $1351\text{ cm}^{-1}$  corresponds to various modes of  $NO_3^-$  anion that overlaps in this region. This wavenumber region from  $1200$  to  $1500\text{ cm}^{-1}$  that is chosen for deconvolution is reflected in the work of Shetty et al. (2021) for the solid polymer electrolyte systems.

Fall of  $NO_3^-$  a peak in the wavenumber region between  $1200$  to  $1500\text{ cm}^{-1}$  has brought about a change in the intensity and band structure. The change that is observed in this region is due to the interaction between  $NO_3^-$  ion via hydrogen bond with the functional group present in the polymer blend. The deconvoluted FTIR spectra consist (Refer to Fig. 5) of 4 bands, the band observed between the wavenumber region  $1323$  to  $1326\text{ cm}^{-1}$  corresponds to the free anions and the band observed at the higher wavenumber

side from  $1399$  to  $1406\text{ cm}^{-1}$  corresponds to contact ion pairs since the energy required to form contact ion pairs is more than that of the free anion, therefore, band at higher wave number corresponds to contact ion pairs (Saadiah et al. 2020).

The percentage of free anions available in the bulk of the poly-blend is evaluated by considering the area under the free anions ( $A_f$ ) and contact ion ( $A_c$ ) peak in the deconvoluted spectra using Eq. (2)

$$\text{Percentage of free anion (\%)} = \frac{A_f}{A_f + A_c} \times 100\% \quad (2)$$

Transport parameters: charge density ( $\eta$ ), Ionic mobility ( $\mu$ ), and diffusion coefficient ( $D$ ) are evaluated from the following Eqs. (3), (5), and (6)

$$\eta = \frac{MN_A}{V_{\text{Total}}} \times \text{free ion(\%)} \quad (3)$$

$$V_{\text{Total}} = \left[ \frac{\text{weight}}{\text{density}}(\text{CH}) \right] + \left[ \frac{\text{weight}}{\text{density}}(\text{MC}) \right] + \left[ \frac{\text{weight}}{\text{density}}(Mg(NO_3)_2 \cdot 6H_2O) \right] \quad (4)$$

$$\mu = \frac{\sigma}{\eta e} \quad (5)$$

$$D = \frac{k_B T \mu}{e} \quad (6)$$

where  $M$  is the number of moles of dopant ( $Mg(NO_3)_2$ ),  $N_A$  is the Avogadro's constant ( $6.02 \times 10^{23}/\text{mol}$ ),  $V_{\text{Total}}$  is the total volume of the SPEs system,  $k_B$  is the Boltzmann constant ( $1.38 \times 10^{-23}\text{ JK}^{-1}$ ),  $T$  is the absolute temperature in Kelvin and  $e$  is the electric charge ( $1.602 \times 10^{-19}\text{ C}$ ).

#### Impedance analysis

The Nyquist plots of pristine and doped PEs are shown in Fig. 6. An inclined spike and a depressed semicircle can be seen in a Nyquist plot of a pure poly-blend sample. (Perumal et al. 2019). The polymer electrolyte's bulk resistance and capacitance cause the high-frequency semicircle, while the free charge accumulation

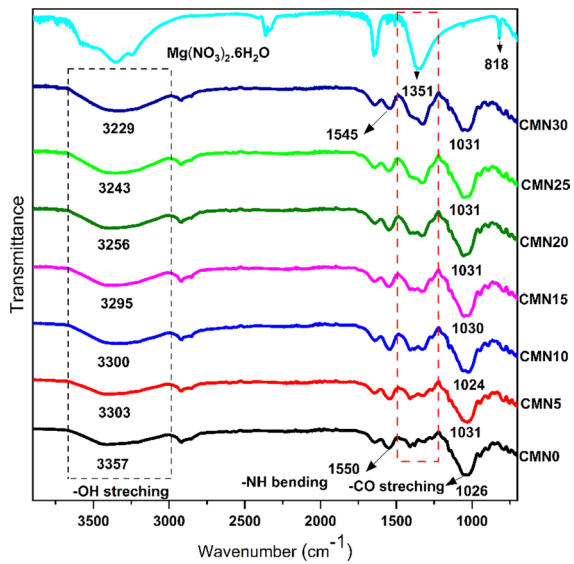
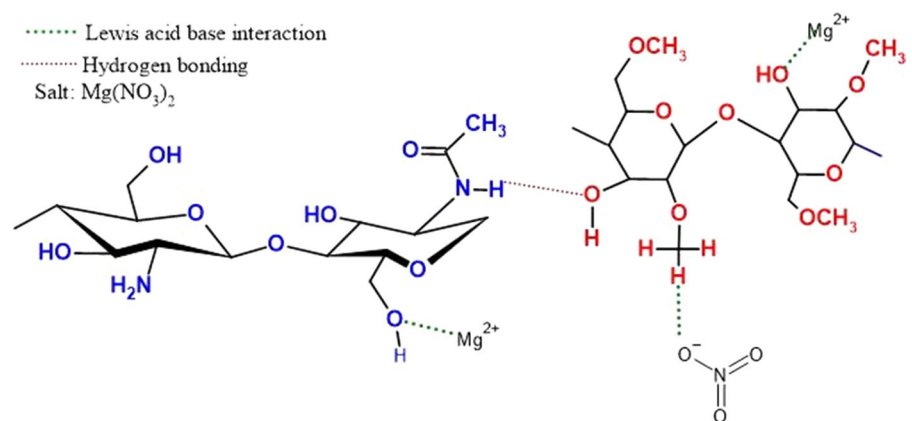


**Fig. 3** FTIR spectrum of magnesium salt, pure blend, and pure blend added with different weight ratios of  $\text{Mg}(\text{NO}_3)_2$  indicating the wavenumber change of the main bands

**Table 2** The FTIR peaks for pristine and  $\text{Mg}(\text{NO}_3)_2$  added poly-blend electrolyte samples

Band Assignment	Wave Number ( $\text{cm}^{-1}$ )						
	CMN0	CMN5	CMN10	CMN15	CMN20	CMN25	CMN30
-OH Stretching	3357	3277	3276	3276	3277	3277	3277
C-H Stretching	2918	2920	2919	2917	2932	2924	2932
C=O Stretching	1641	1639	1641	1640	1640	1640	1649
-NH Bending	1550	1550	1549	1545	1544	1550	1550
C-O Bending	1057	1058	1058	1058	1058	1061	1057
C-O Stretching	1026	1024	1024	1024	1024	1021	1021

**Fig. 4** Possible Interaction scheme of  $\text{Mg}(\text{NO}_3)_2$  with the poly-blend CS:MC



at the electrode/electrolyte interface causes the low-frequency spike's blocking capacitance (Pritam et al. 2019). In our study, a high-frequency semicircle and a low-frequency non-vertical spike have been observed for the biopolymer electrolyte CMN0 and all other compositions of poly-blend with different concentrations of  $\text{Mg}(\text{NO}_3)_2$  salt (Kiruthika et al. 2020). The high-frequency semicircle presents bulk conductance, equivalent to the parallel combination of bulk resistance ( $R_b$ ) and bulk capacitance of the PE (Abdulkaareem 2021). While the low-frequency region exhibits behavior similar to a constant phase element (CPE), the high-frequency region exhibits an association of bulk resistance and bulk capacitance [2]. The leaky capacitor and CPE are analogous. The depressed semicircle can be explained through the CPE rather than a capacitor, and the low-frequency tail is introduced as another CPE. A resistor is described as the migration of the  $\text{Mg}^{2+}$  ion, whereas a capacitor is the immovable



polymer backbone chain that polarizes in the alternating field (Rani et al. 2015; Sowthari and Suthanthiraraj 2013).

Impedance analysis was carried out to arrive at the ionic conductivity ( $\sigma$ ) of the poly-blend system using the relation (7)

$$(\sigma) = \frac{t}{R_b A} \quad (7)$$

where  $t$  is the thickness of the film,  $A$  is the contact area of the sample with the electrode and  $R_b$  is the bulk resistance of the sample that is obtained by fitting the Nyquist plot using EIS spectrum analyzer software (Bondarenko 2005) with less than 10% error using an equivalent circuit as depicted in Fig. 6.

A clear picture of ionic conductivity correlation with transport parameters is understandable from Fig. 7. Charge carrier density ( $\eta$ ) increased with increased salt concentration, indicating the dissociation of salt by the functional group of the polymer. Direct correlation of  $\eta$  with conductivity ( $\sigma \propto \eta$ ) was not observed due to a fall of ionic conductivity in the case of CMN10 and CMN25 samples and is due to a decrease in ionic mobility and diffusivity as per the transport parameters calculated from FTIR deconvolution technique and justified due to increase in crystallinity that may hinder the motion of ions in the SBPE system. CMN20 sample exhibited the highest diffusion coefficient and mobility and is due to a decrease in crystallinity due to polymer-ion interaction. From impedance spectroscopy analysis, it has been found that the SBPE CMN30 has the highest ionic conductivity value of  $2.12 \times 10^{-5} \text{ Scm}^{-1}$ .

Frequency-dependent study of conductivity:

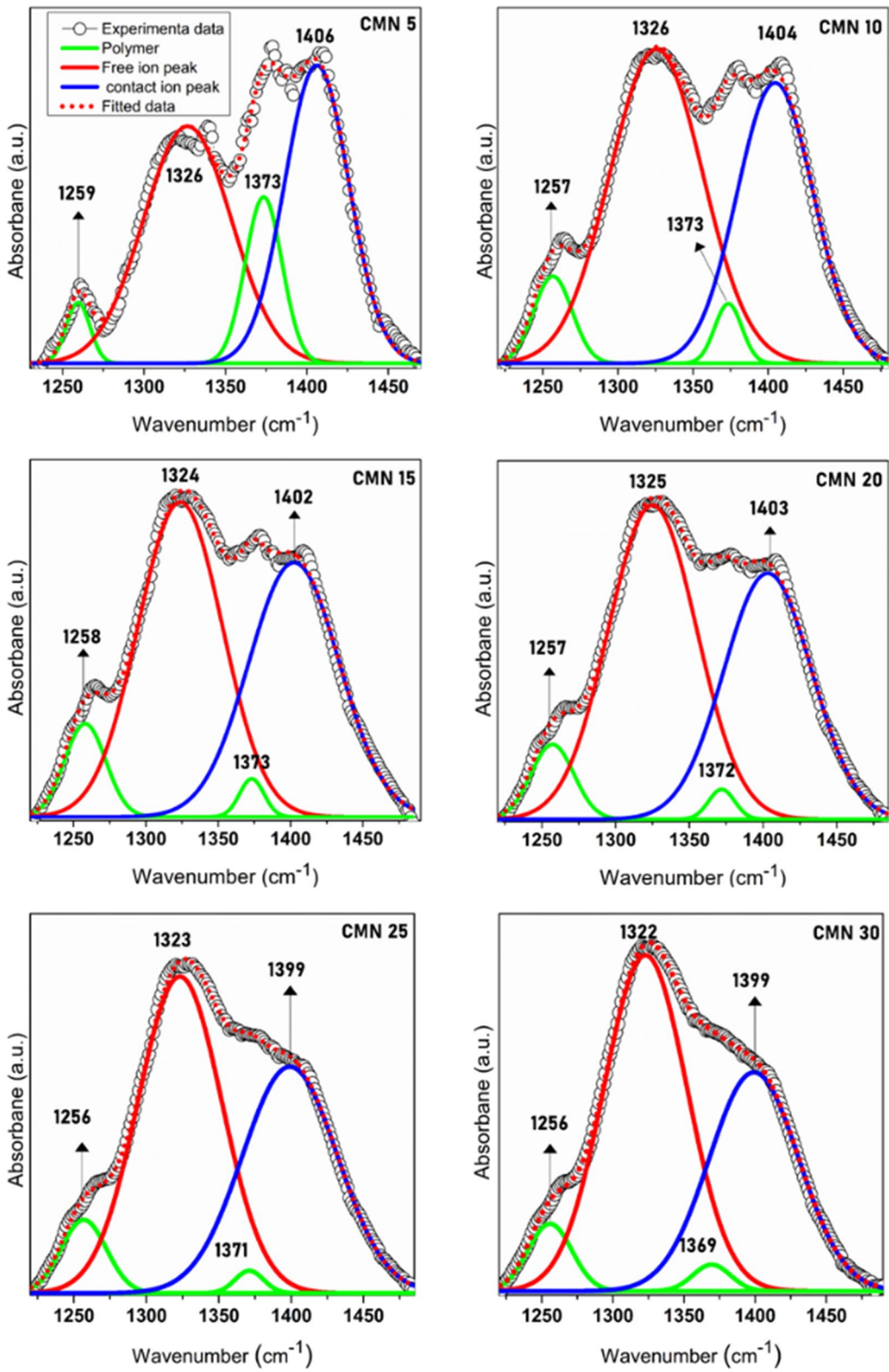
Figure 8 shows the frequency-dependent ac conductivity of the SBPE with various amounts of  $\text{Mg}(\text{NO}_3)_2$ . The below Fig. 8 shows three distinct regions, that is, low-frequency dispersion region which shows the space charge polarization at the blocking electrode, a middle-frequency independent plateau region showing the DC conductivity of the prepared SBPE due to ion migration to neighboring sites and the high-frequency region which indicates the bulk relaxation process (Rathika and Suthanthiraraj 2016).

SEM analysis

SEM images can be used as an effective tool to gain information about the morphological aspects of the solid polymer electrolyte samples. The SEM micrographs of the pure blend and blend doped with various concentration of  $\text{Mg}(\text{NO}_3)_2$  salt is shown in Fig. 9. The detection of phase separations and interfaces using SEM has been widely used to investigate the compatibility between different components of blended polymer electrolytes. CMN0 has smooth surface morphology due to the absence of salt in the blend matrix. CMN5 and CMN10 are almost similar with an intergranular appearance on the surface without any phase separation. While in CMN15 and CMN20 with the increase in salt concentration there might be an increase in the interaction of salt with polymer chains, hence the occurrence of pores on the surface can be observed. These pores facilitate the movement of ions and segmental motion of the polymer matrix (Yap et al. 2013), hence the crystallinity decreased, as depicted in XRD studies. Furthermore, with the increase in salt concentration (CMN25 and 30) the surface was wrinkled and has minute pores indicating enhanced interaction between them. Moreover, in all the salt-containing blends as there is no agglomeration of salt on the surface of the blend electrolyte systems, the smooth surface aids the free transfer of ions within the polymer matrix and is similar to enhanced number density data (Abdulkareem 2021).

I-V Characterization

The ESW of the SBPE samples has been studied and the I-V plot of the same is shown in Fig. 10. The current begins to progressively increase as the potential increases. The ESW of the SBPE samples has been calculated and presented in Table 3. It was found that the ESW gradually raises and reaches a maximum value of 3.65 V for 30 wt.% of  $\text{Mg}(\text{NO}_3)_2$ . This implies that the magnesium-ion conducting SBPE system is electrochemically stable up to 3.65 V, which is an acceptable range for use in magnesium-ion primary batteries (Manjuladevi et al. 2018a). The maximum ESW of 2.05 V was



◀**Fig. 5** FTIR deconvolution of  $CH : MC : Mg(NO_3)_2$  electrolyte system in 1200–1500  $cm^{-1}$  region

obtained for the SBPE based on pectin with  $MgCl_2$  reported by Kiruthika et al. (2020), Manjuladevi et al. (2018a) reported a stability window of 3.4 V for the PVA: PAN blend with magnesium nitrate as a salt. The obtained ESW value is better than the reported values.

#### Transference number measurement (TNM)

Studying the TNM is essential to employ the SBPE in device applications. A TNM investigation is used to determine the dominant charge carrier species (Manjuladevi et al. 2017). The total ion and electron transference numbers can be calculated using the following equations:

$$t_{ion} = \frac{I_i - I_{ss}}{I_i} \quad (8)$$

$$t_{ele} = 1 - t_{ion} \quad (9)$$

where  $I_i$  is the starting current and  $I_{ss}$  is the steady-state current (Polu et al. 2015).

Figure 11 shows the electrolyte polarization at 0.5 V. At first, both the ion and the electron cause a significant current value. The electrodes were made of SS, which is known to block ions, so the current value decreased noticeably before stabilizing (Aziz et al. 2019). The highest conducting SBPE's total ion transport number was found to be 0.86. It was found that ions were the dominant charge carriers (Ponmani et al. 2018; Polu et al. 2012).

#### Cyclic voltammogram (CV) studies

For use in Mg batteries, the electrochemical reversibility of  $Mg/Mg^{2+}$  from an SBPE needs to be thoroughly studied. The following two symmetrical cells were subjected to CV measurements using SBPE with 30 wt.% of  $Mg(NO_3)_2$ .

First cell: SS/CMN30/SS.

Second cell: Mg/CMN30/Mg.

Figures 12 (a) and (b) show the first cell's and second cell's CV plots, which were obtained at a scanning rate of  $100 \text{ mVs}^{-1}$ . The CV trace shows a distinct cathodic and anodic peak for the second cell, while the first cell does not have such peaks (Fig. 12). The first cell has a higher current magnitude than the second cell. The second cell CV also displays an anodic peak and a minor cathodic peak. This shows that cathodic deposition and anodic magnesium dissolution at the electrode/electrolyte interface occur in the second cell. This confirms the compatibility of Mg ions in the prepared SBPE (Cyriac et al. 2022).

#### Study of Mg ion primary battery

To study the practical applicability of these polymer electrolytes for primary batteries, a primary magnesium ion battery is built by incorporating the highest conducting sample i.e., CMN30 as the electrolyte in between the magnesium metal pellet (anode) and cathode materials using the battery holder. Choosing the anode materials in solid-state batteries depends on the mobile species in the electrolyte (Radhakrishna 1990). In this work, a magnesium metal pellet is used as an anode material. To study the influence of electrode material on the performance of the battery, we have chosen two types of cathode materials. One of the cell systems is  $Mg/CMN30/(I_2 + C + CMN30)$  designated as cell 1 and the other one is  $Mg/CMN30/(MnO_2 + C)$  designated as cell 2. In cell 1, iodine plays the role of "active cathode." Having graphite increases the cathode material's electronic conductivity (Rao et al. 2012). With the addition of polymer electrolytes, the cathode mixture has a larger surface area for interfacial contact, which lowers interfacial resistance and improves battery performance (Austin 1973). The cell parameters are listed in Table 4. In cell 1, an initial OCV of 1.66 V (Refer to Fig. 13a) was reduced to 1.50 V and maintained the same for 24 h. After connecting a load of 100 k $\Omega$ , the voltage of 1.50 V was reduced to 1.03 V during the time duration of 24 h. Initially, 1.2 V is maintained constant for 12 h, and this constant region is called the plateau region. In Cell 2 (Refer Fig. 13b), an initial OCV of 1.92 V was reduced to 1.80 V and maintained the same for 24 h. After connecting a load of 100 k $\Omega$ ,

**Fig. 6** Nyquist plot for pristine poly-blend and poly-blend doped with magnesium salt

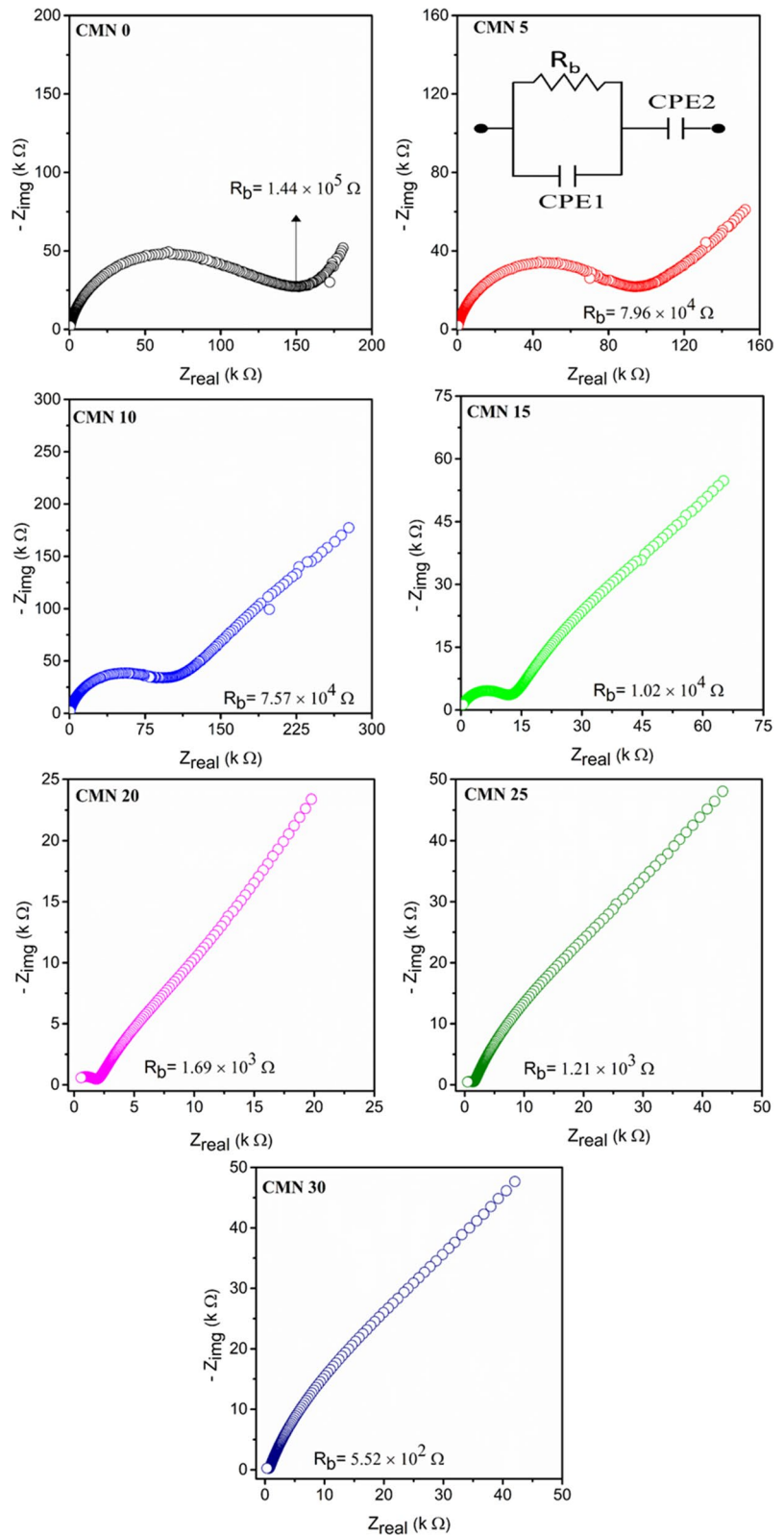


**Fig. 7** Variation of ionic conductivity ( $\sigma$ ) (error bars shown as vertical lines within the data points), charge carrier concentration ( $\eta$ ), mobility ( $\mu$ ), and diffusion coefficient ( $D$ ) with salt concentration

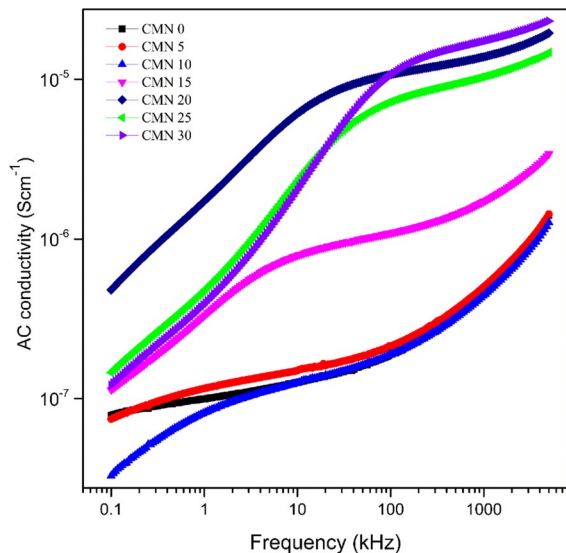
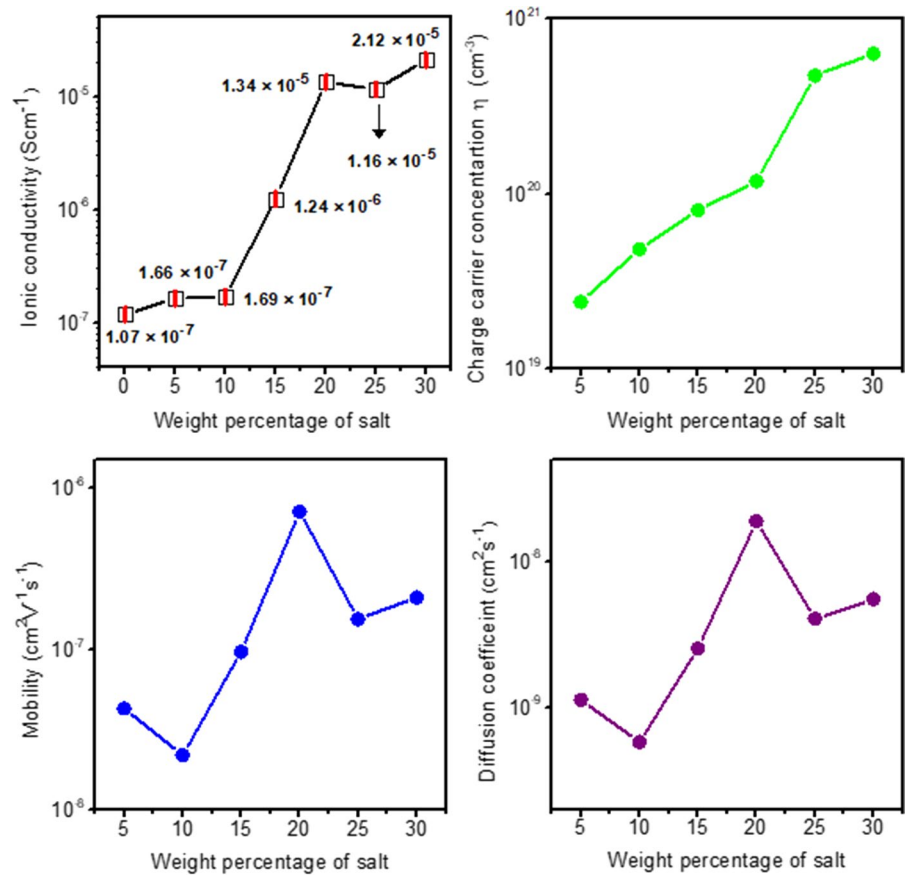
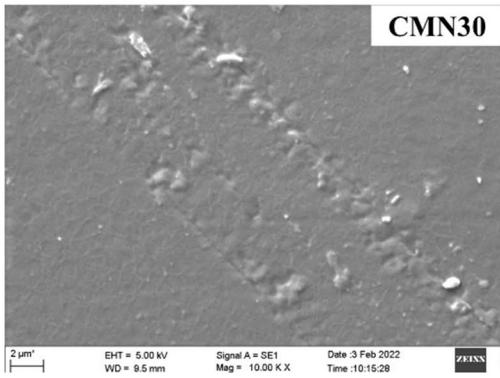
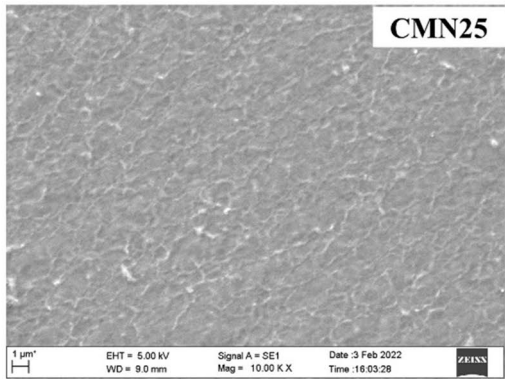
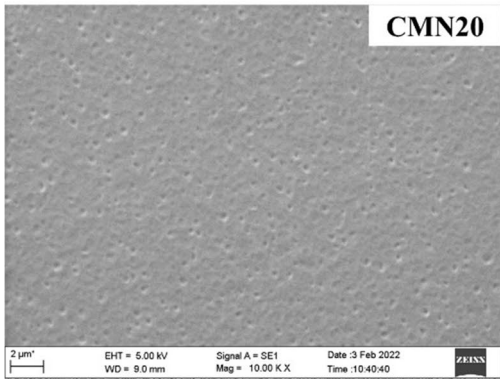
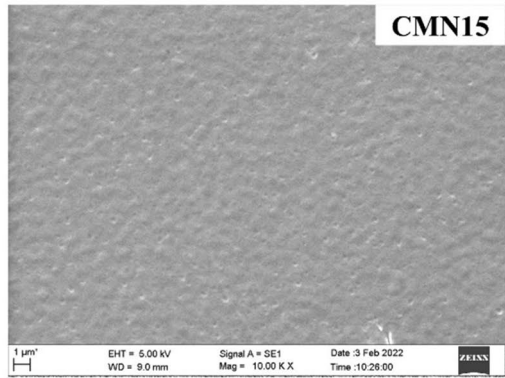
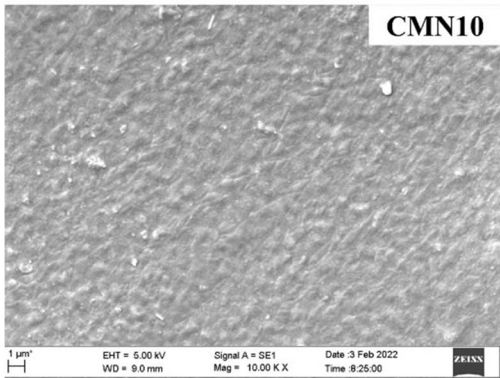
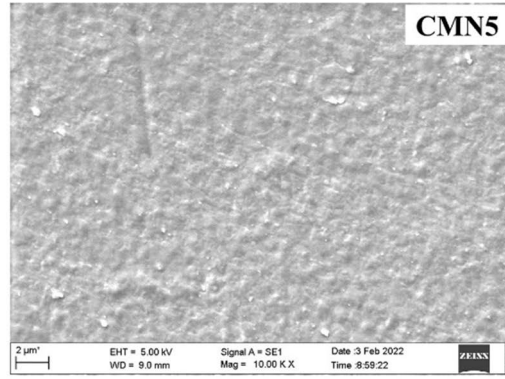
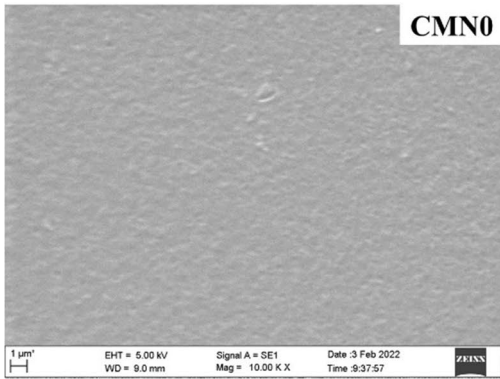


**Fig. 8** Frequency-dependent ac conductivity of pure and salt doped blend electrolyte

the voltage of 1.80 V was reduced to 0.89 V during the time duration of 10 h. The first rapid drop in cell voltage may have been due to polarization or the formation of a thin layer of magnesium salt at the electrode/electrolyte interface (Polu and Kumar 2013). As indicated in Table 5, the findings of the current investigation are comparable to those of earlier studies. The performance of the cell 1 is better than the cell 2 because the discharge time for plateau region of cell 1 is around 12 to 13 h whereas that of cell 2 is only 8 to 9 h. This indicates that the present polymer electrolyte may be used in solid-state batteries.







◀**Fig. 9** SEM images of pristine poly-blend and poly-blend incorporated with various amounts of  $\text{Mg}(\text{NO}_3)_2$  salt

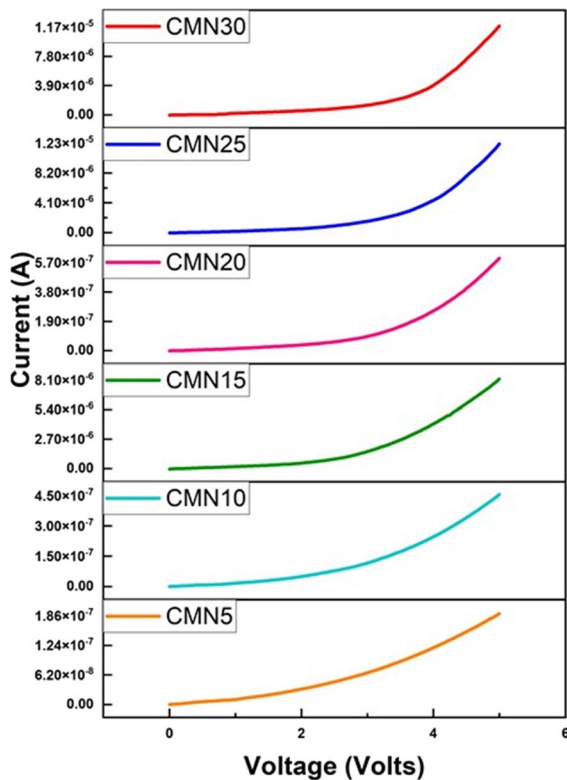


**Fig. 10** Current to voltage graph for the cell constructed with stainless steel (SS)/[CS: MC]:  $\text{Mg}(\text{NO}_3)_2$ /stainless steel (SS)

**Table 3** ESW and  $t_{\text{ion}}$  of the prepared SBPE films

Polyblend electrolyte	ESW (V)	$t_{\text{ion}}$
CMN5	2.49	0.86
CMN10	2.97	0.90
CMN15	3.12	0.82
CMN20	3.45	0.83
CMN25	3.61	0.71
CMN30	3.65	0.86

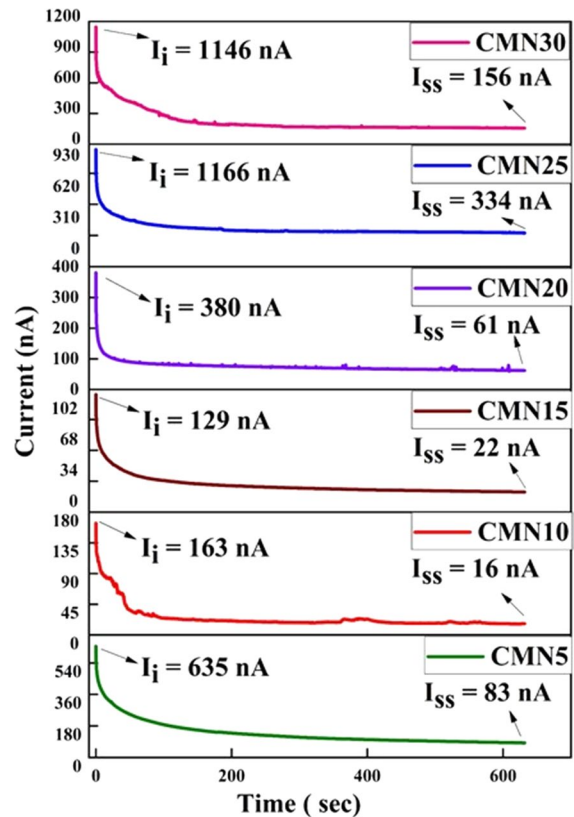


**Fig. 11** Transference number of electrolytes

## Conclusions

The solution casting approach was employed to synthesize the SBPE using CS:MC with the varied quantity of  $\text{Mg}(\text{NO}_3)_2$ . CS and MC were used as the biopolymer blend matrix where ions provided by  $\text{Mg}(\text{NO}_3)_2$  participate in the conduction process. The XRD analysis reveals that the prepared polymer electrolyte was amorphous in nature. FTIR study validates the complex formation between the biopolymer and the magnesium nitrate salt. From EIS analysis, it has been found that 30 wt.% magnesium nitrate added sample, i.e., CMN30, exhibits the highest ionic conductivity of  $2.12 \times 10^{-5} \text{ Scm}^{-1}$  at room temperature. The

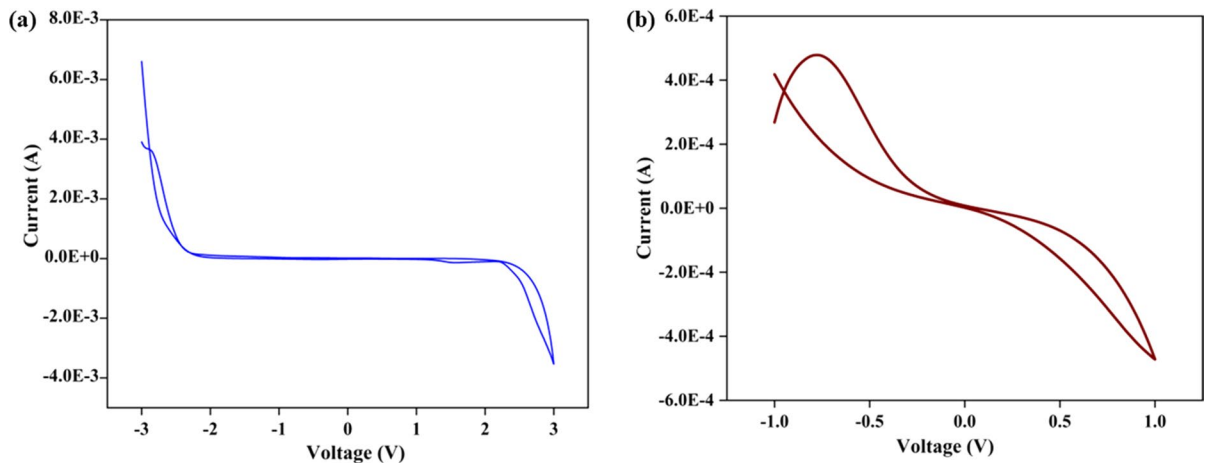


**Fig. 12** CV of (a) SS/CMN30/SS and (b) Mg/CMN30/Mg SBPE at a scan rate of  $100 \text{ mVs}^{-1}$

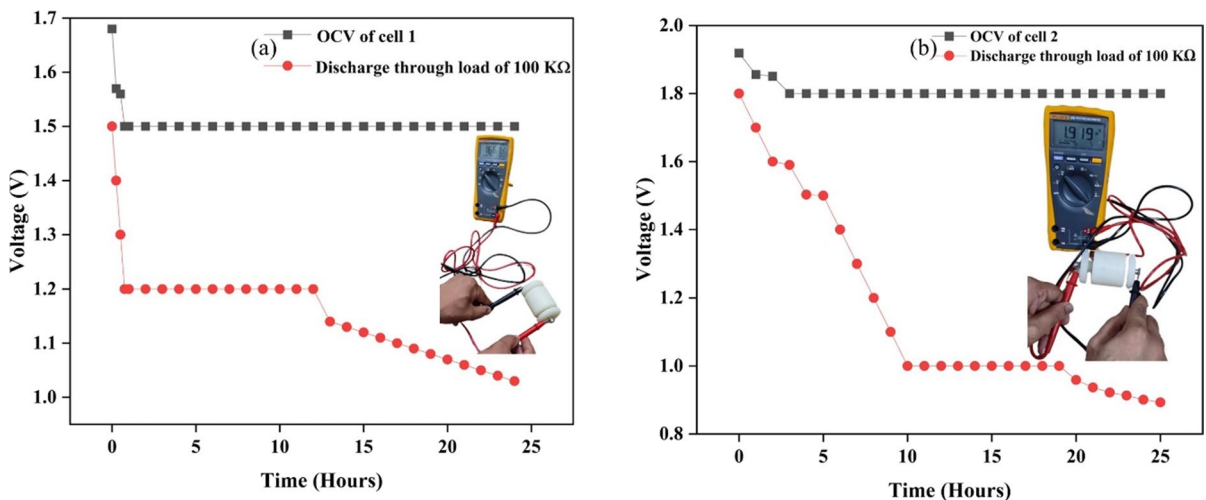


**Fig. 13** (a) OCV of cell 1 (inset shows photo image of cell 1), (b) OCV of cell 2 (inset shows photo image of cell 2)

**Table 4** Parameters of the cell

Parameter	Measured values	
	Cell 1	Cell 2
Area of the cell ( $\text{cm}^2$ )	1.23	1.23
Effective diameter of the cell (cm)	1.30	1.30
Thickness of the cell (cm)	0.45	0.56
Weight of the cell (g)	1.36	1.59
OCV (V)	1.66	1.92

electrochemical stability for the highest conducting sample is found to be 3.65 V which is sufficient for practical applications in electrochemical devices such as a battery. The total ionic transference number of the highest conducting electrolyte was 0.86. The magnesium ion electrochemical cells assembled using the CMN30 SBPE membrane which acts both as an electrolyte and separator show an open circuit voltage of 1.92 V at room temperature. Thus CS:MC:Mg(NO<sub>3</sub>)<sub>2</sub> system demonstrates as

**Table 5** Comparison of the OCV obtained in the present work with the previous studies using the magnesium metal as an anode

Electrolyte	Cathode	OCV	Reference
PVA + PAN + Mg(NO <sub>3</sub> ) <sub>2</sub>	MnO <sub>2</sub> + C	2.02	(Manjuladevi et al. 2018a)
Pectin + MgCl <sub>2</sub>	MnO <sub>2</sub> + C	2.16	(Kiruthika et al. 2020)
PVA + PAN + Mg(ClO <sub>4</sub> ) <sub>2</sub>	MnO <sub>2</sub>	2.06	(Mahalakshmi et al. 2020)
PVA + PEG + Mg(CH <sub>3</sub> COO) <sub>2</sub>	I <sub>2</sub> + C + Electrolyte	1.84	(Manjuladevi et al. 2017)
I-carrageenan + Mg (NO <sub>3</sub> ) <sub>2</sub>	MnO <sub>2</sub> + C + Electrolyte	2.08	(Manjuladevi et al. 2018b)
<b>MC + CS + Mg(NO<sub>3</sub>)<sub>2</sub></b>	<b>MnO<sub>2</sub> + C</b>	<b>1.92</b>	<b>Present work</b>
<b>MC + CS + Mg(NO<sub>3</sub>)<sub>2</sub></b>	<b>I<sub>2</sub> + C + Electrolyte</b>	<b>1.66</b>	<b>Present work</b>

an efficient SBPE for the futuristic magnesium ion batteries.

**Acknowledgements** One of the authors Pradeep Nayak acknowledges the financial assistance from the “University Grants Commission, New Delhi, Government of India” in the form of “Junior Research Fellowship”, sanction order: 1237/ (CSIR-UGC NET DEC. 2017) dated 21-01-2019.

**Authors’ contributions** PN: Conceptualization, Methodology, Data curation, Investigation, Writing-Original draft preparation. YNS: Visualization, Resources, Data curation, Investigation. SD: Resources. I: Methodology, Investigation, Validation, Resources, Supervision. SKS: Formal analysis, Validation. VC: Formal analysis, Writing- Reviewing and Editing.

**Funding** Open access funding provided by Manipal Academy of Higher Education, Manipal. Pradeep Nayak has received funding from University Grants Commission (UGC), New Delhi, Government of India as Junior Research Fellowship (JRF) with sanction number UGC-Ref. No. 1237/ (CSIR-UGC NET DEC. 2017) dated 21–01-2019.

**Data availability** No data or material is provided with this manuscript.

#### Declarations

**Conflict of interests** The authors declare that they have no known competing financial interests or personal relationships that could have appeared to influence the work reported in this paper.

**Consent for publication** The authors hereby consent to publication of the present research work in this journal, if selected for publication.

**Ethics approval** This article does not contain any studies with human participants or animals performed by any of the authors.

**Open Access** This article is licensed under a Creative Commons Attribution 4.0 International License, which permits use, sharing, adaptation, distribution and reproduction in any medium or format, as long as you give appropriate credit to the original author(s) and the source, provide a link to the Creative Commons licence, and indicate if changes were made. The

images or other third party material in this article are included in the article’s Creative Commons licence, unless indicated otherwise in a credit line to the material. If material is not included in the article’s Creative Commons licence and your intended use is not permitted by statutory regulation or exceeds the permitted use, you will need to obtain permission directly from the copyright holder. To view a copy of this licence, visit <http://creativecommons.org/licenses/by/4.0/>.

#### References

- Abdulkareem SS (2021) Structural, morphological and electrical properties of chitosan/methylcellulose blend polymer doped with different concentrations of NH<sub>4</sub>NO<sub>3</sub>. *Mater Res Express*. <https://doi.org/10.1088/2053-1591/ac1d69>
- Abdullah OGH, Hanna RR, Salman YAK (2019) Structural and electrical conductivity of CH:MC bio-poly-blend films: optimize the perfect composition of the blend system. *Bull Mater Sci* 42:1–7. <https://doi.org/10.1007/s12034-019-1742-3>
- Abdullah AM, Aziz SB, Saeed SR (2021) Structural and electrical properties of polyvinyl alcohol (PVA): methyl cellulose (MC) based solid polymer blend electrolytes inserted with sodium iodide (NaI) salt. *Arab J Chem* 14:103388. <https://doi.org/10.1016/j.arabj.2021.103388>
- Abdullah OG, Hanna RR, Ahmed HT et al (2021) Conductivity and dielectric properties of lithium-ion biopolymer blend electrolyte based film. *Results Phys* 24:104135. <https://doi.org/10.1016/j.rinp.2021.104135>
- Arya A, Sharma AL (2019) Electrolyte for energy storage/conversion (Li<sup>+</sup>, Na<sup>+</sup>, Mg<sup>2+</sup>) devices based on PVC and their associated polymer: a comprehensive review. *J Solid State Electrochem* 23:997–1059. <https://doi.org/10.1007/s10008-019-04203-x>
- Austin LG (1973) *Techn ca]l Notes*. 120:4–7
- Aziz SB, Abdullah OG, Hussein SA, Ahmed HM (2017) Effect of PVA blending on structural and ion transport properties of CS: AgNt-based polymer electrolyte membrane. *Polymers (Basel)*. <https://doi.org/10.3390/polym9110622>
- Aziz SB, Hamsan MH, Abdullah RM, Kadir MFZ (2019) A promising polymer blend electrolytes based on chitosan: Methyl cellulose for EDLC application with high specific capacitance and energy density. *Molecules*. <https://doi.org/10.3390/molecules24132503>

- Aziz SB, Brevik I, Hamsan MH et al (2020a) Compatible solid polymer electrolyte based on methyl cellulose for energy storage application: Structural, electrical, and electrochemical properties. *Polymers (basel)* 12:1–19. <https://doi.org/10.3390/polym12102257>
- Aziz SB, Hamsan MH, Abdullah RM, Abdulwahid RT, Brza MA, Marif AS, Kadir MFZ (2020b) Protonic EDLC cell based chitosan methylcellulose solid Polym blend electrolytes. *Ionics* 26(4):1829–1840. <https://doi.org/10.1007/s11581-020-03498-5>
- Aziz SB, Hamsan MH, Nofal MM et al (2020c) From cellulose, shrimp and crab shells to energy storage EDLC cells: the study of structural and electrochemical properties of proton conducting chitosan-based biopolymer blend electrolytes. *Polymers (basel)* 12:1–24. <https://doi.org/10.3390/polym12071526>
- Aziz SB, Asnawi ASFM, Kadir MFZ et al (2021) Structural, electrical and electrochemical properties of glycerolized biopolymers based on chitosan (Cs): methylcellulose (mc) for energy storage application. *Polymers (Basel)*. <https://doi.org/10.3390/polym13081183>
- Bdewi SF, Abdullah OG, Aziz BK, Mutar AAR (2016) Synthesis, structural and optical characterization of MgO nanocrystalline embedded in PVA matrix. *J Inorg Organomet Polym Mater* 26:326–334. <https://doi.org/10.1007/s10904-015-0321-3>
- Bondarenko AS RGA (2005) No Title. 89–102
- Buraidah MH, Arof AK (2011) Characterization of chitosan/PVA blended electrolyte doped with  $\text{NH}_4\text{I}$ . *J Non Cryst Solids* 357:3261–3266. <https://doi.org/10.1016/j.jnoncryst.2011.05.021>
- Cyriac V, Ismayil NIM et al (2022) Ionic conductivity enhancement of PVA: carboxymethyl cellulose polyblend electrolyte films through the doping of NaI salt. *Cellulose* 29:3271–3291. <https://doi.org/10.1007/s10570-022-04483-z>
- Dannoun EMA, Aziz SB, Brza MA et al (2020) The study of plasticized solid polymer blend electrolytes based on natural polymers and their application for energy storage EDLC devices. *Polymers (basel)* 12:1–19. <https://doi.org/10.3390/polym12112531>
- Graham M, Shchukina E, De Castro PF, Shchukin D (2016) Nanocapsules containing salt hydrate phase change materials for thermal energy storage. *J Mater Chem A* 4:16906–16912. <https://doi.org/10.1039/c6ta06189c>
- Jeyabanu K, Siva V, Nallamuthu N et al (2018) Investigation of electrochemical studies of magnesium ion conducting poly(vinyl alcohol)–poly(vinyl pyrrolidone) based blend polymers. *J Nanosci Nanotechnol* 18:1103–1109. <https://doi.org/10.1166/jnn.2018.13969>
- Kadir MFZ, Aspanut Z, Majid SR, Arof AK (2011) FTIR studies of plasticized poly(vinyl alcohol)-chitosan blend doped with  $\text{NH}_4\text{NO}_3$  polymer electrolyte membrane. *Spectrochim Acta Part A Mol Biomol Spectrosc* 78:1068–1074. <https://doi.org/10.1016/j.saa.2010.12.051>
- Kanimozhi K, Khaleel Basha S, Sugantha Kumari V (2016) Processing and characterization of chitosan/PVA and methylcellulose porous scaffolds for tissue engineering. *Mater Sci Eng C* 61:484–491. <https://doi.org/10.1016/j.msec.2015.12.084>
- Kesavan K, Mathew CM, Rajendran S et al (2015) Solid polymer blend electrolyte based on poly(ethylene oxide) and poly(vinyl pyrrolidone) for lithium secondary batteries. *Brazilian J Phys* 45:19–27. <https://doi.org/10.1007/s13538-014-0279-6>
- Khair ASA (2018) Electrical and structural studies of polymer electrolyte based on 2 chitosan/ methyl cellulose blend doped with BMIMTFSI. *Mater Res Express*. <https://doi.org/10.1088/2053-1591/aac25b>
- Kiruthika S, Malathi M, Selvasekarapandian S et al (2020) Conducting biopolymer electrolyte based on pectin with magnesium chloride salt for magnesium battery application. *Polym Bull* 77:6299–6317. <https://doi.org/10.1007/s00289-019-03071-9>
- Kumar M, Tiwari T, Chauhan JK, Srivastava N (2015) Understanding the ion dynamics and relaxation behavior from impedance spectroscopy of NaI doped zwitterionic polymer system. *Mater Res Express*. <https://doi.org/10.1088/2053-1591/1/4/045003>
- Kumari VS, Basha SK, Sudha PN (2012) Physicochemical and morphological evaluation of chitosan/poly(vinyl alcohol)/methylcellulose chemically cross-linked ternary blends. *Polym Bull* 68:1387–1393. <https://doi.org/10.1007/s00289-011-0645-2>
- Lawrie G, Keen I, Drew B et al (2007) Interactions between alginate and chitosan biopolymers characterized using FTIR and XPS. *Biomacromol* 8:2533–2541. <https://doi.org/10.1021/bm070014y>
- Liu PT, Wei XM, Liu Z (2013) Miscibility study of chitosan and methylcellulose blends. *Adv Mater Res* 750–752:802–805. <https://doi.org/10.4028/www.scientific.net/AMR.750-752.802>
- Mahalakshmi M, Selvanayagam S, Selvasekarapandian S et al (2020) Magnesium ion-conducting solid polymer electrolyte based on cellulose acetate with magnesium nitrate ( $\text{Mg}(\text{NO}_3)_2 \cdot 6\text{H}_2\text{O}$ ) for electrochemical studies. *Ionics (kiel)* 26:4553–4565. <https://doi.org/10.1007/s11581-020-03615-4>
- Manjuladevi R, Thamilselvan M, Selvasekarapandian S et al (2017) Mg-ion conducting blend polymer electrolyte based on poly(vinyl alcohol)-poly (acrylonitrile) with magnesium perchlorate. *Solid State Ionics* 308:90–100. <https://doi.org/10.1016/j.ssi.2017.06.002>
- Manjuladevi R, Selvasekarapandian S, Thamilselvan M et al (2018a) A study on blend polymer electrolyte based on poly(vinyl alcohol)-poly (acrylonitrile) with magnesium nitrate for magnesium battery. *Ionics (kiel)* 24:3493–3506. <https://doi.org/10.1007/s11581-018-2500-z>
- Manjuladevi R, Thamilselvan M, Selvasekarapandian S et al (2018b) Preparation and characterization of blend polymer electrolyte film based on poly(vinyl alcohol)-poly(acrylonitrile)/ $\text{MgCl}_2$  for energy storage devices. *Ionics (kiel)* 24:1083–1095. <https://doi.org/10.1007/s11581-017-2273-9>
- Mazuki NF, Rasali NMJ, Saadiah MA, Samsudin AS (2018) Irregularities trend in electrical conductivity of CMC/PVA- $\text{NH}_4\text{Cl}$  based solid biopolymer electrolytes. *AIP Conf Proc* 10(1063):5066862
- Nadirah BN, Ong CC, Saheed MSM et al (2020) Structural and conductivity studies of polyacrylonitrile/methylcellulose

- blend based electrolytes embedded with lithium iodide. *Int J Hydrogen Energy* 45:19590–19600. <https://doi.org/10.1016/j.ijhydene.2020.05.016>
- Nayak P, Cyriac V, Hegde S, Sanjeev G (2022) Magnesium ion conducting free-standing biopolymer blend electrolyte films for electrochemical device application. *J Non Cryst Solids* 592:121741. <https://doi.org/10.1016/j.jnoncrsol.2022.121741>
- Perumal P, Abhilash KP, Sivaraj P, Selvin PC (2019) Study on Mg-ion conducting solid biopolymer electrolytes based on tamarind seed polysaccharide for magnesium ion batteries. *Mater Res Bull* 118:110490. <https://doi.org/10.1016/j.materresbull.2019.05.015>
- Polu AR, Kumar R (2013) Preparation and characterization of pva based solid polymer electrolytes for electrochemical cell applications. *Chin J Polym Sci Eng Ed* 31:641–648. <https://doi.org/10.1007/s10118-013-1246-3>
- Polu AR, Kumar R, Kumar KV (2012) Ionic conductivity and electrochemical cell studies of new Mg<sup>2+</sup> ion conducting PVA/PEG based polymer blend electrolytes. *Adv Mater Lett* 3:406–409. <https://doi.org/10.5185/amlett.2012.6375>
- Polu AR, Kumar R, Rhee HW (2015) Magnesium ion conducting solid polymer blend electrolyte based on biodegradable polymers and application in solid-state batteries. *Ionics (kiel)* 21:125–132. <https://doi.org/10.1007/s11581-014-1174-4>
- Ponmani S, Kalaiselvi J, Ramesh Prabhu M (2018) Structural, electrical, and electrochemical properties of poly(vinylidene fluoride-co-hexafluoropropylene)/poly(vinyl acetate)-based polymer blend electrolytes for rechargeable magnesium ion batteries. *J Solid State Electrochem* 22:2605–2615. <https://doi.org/10.1007/s10008-018-3971-6>
- Pritam AA, Sharma AL (2019) Dielectric relaxations and transport properties parameter analysis of novel blended solid polymer electrolyte for sodium-ion rechargeable batteries. *J Mater Sci* 54:7131–7155. <https://doi.org/10.1007/s10853-019-03381-3>
- Rani MSA, Mohamed NS, Isa MIN (2015) Investigation of the ionic conduction mechanism in carboxymethyl cellulose/chitosan biopolymer blend electrolyte impregnated with ammonium nitrate. *Int J Polym Anal Charact* 20:491–503. <https://doi.org/10.1080/1023666X.2015.1050803>
- Rao CVS, Ravi M, Raja V et al (2012) Preparation and characterization of PVP-based polymer electrolytes for solid-state battery applications. *Iran Polym J Engl Ed* 21:531–536. <https://doi.org/10.1007/s13726-012-0058-6>
- Rathika R, Suthanthiraraj SA (2016) Ionic interactions and dielectric relaxation of PEO/PVDF-Mg[(CF<sub>3</sub>SO<sub>2</sub>)<sub>2</sub>N<sub>2</sub>] blend electrolytes for magnesium ion rechargeable batteries. *Macromol Res* 24:422–428. <https://doi.org/10.1007/s13233-016-4053-1>
- Saadiah MA, Nagao Y, Samsudin AS (2020) Proton (H<sup>+</sup>) transport properties of CMC–PVA blended polymer solid electrolyte doped with NH<sub>4</sub>NO<sub>3</sub>. *Int J Hydrogen Energy* 45:14880–14896. <https://doi.org/10.1016/j.ijhydene.2020.03.213>
- Salman YAK, Abdullah OG, Hanna RR, Aziz SB (2018) Conductivity and electrical properties of chitosan - methylcellulose blend biopolymer electrolyte incorporated with lithium tetrafluoroborate. *Int J Electrochem Sci* 13:3185–3199. <https://doi.org/10.20964/2018.04.25>
- Sarma RVGK, Radhakrishna S (1990) Silver borotungstate glasses: new electrolyte for solid state electrochemical cell. *Solid State Ionics* 204:483–486. [https://doi.org/10.1016/0167-2738\(90\)90385-5](https://doi.org/10.1016/0167-2738(90)90385-5)
- Shetty SK, Ismayil HS et al (2021) Dielectric relaxations and ion transport study of NaCMC:NaNO<sub>3</sub> solid polymer electrolyte films. *Ionics (kiel)* 27:2509–2525. <https://doi.org/10.1007/s11581-021-04023-y>
- Sownthari K, Suthanthiraraj SA (2013) Synthesis and characterization of an electrolyte system based on a biodegradable polymer. *Express Polym Lett* 7:495–504. <https://doi.org/10.3144/expresspolymlett.2013.46>
- Wang J, Song S, Gao S et al (2017) Mg-ion conducting gel polymer electrolyte membranes containing biodegradable chitosan: preparation, structural, electrical and electrochemical properties. *Polym Test* 62:278–286. <https://doi.org/10.1016/j.polymertesting.2017.07.016>
- Wojdyr M, Gierlotka S, Palosz B (2004) FITYK – peak-fitting software with support for powder patterns analysis. *Acta Crystallogr Sect A Found Crystallogr* 60:s246–s246. <https://doi.org/10.1107/s010876730409511x>
- Yap YL, You AH, Teo LL, Hanapei H (2013) Inorganic filler sizes effect on ionic conductivity in polyethylene oxide (PEO) composite polymer electrolyte. *Int J Electrochem Sci* 8:2154–2163

**Publisher's Note** Springer Nature remains neutral with regard to jurisdictional claims in published maps and institutional affiliations.